# Method of applying temperature-sensitive paint in hypersonic test with strong combustion radiation

Chaokai Yuan[1,2], Fanzhao Meng[1,2], Xu Liu[3], Yunfeng Liu[1,2],
Huan Lian[1,2], Yingzheng Liu[3], and Di Peng[3*]

[1]*Institute of Mechanics, Chinese Academy of Sciences, Beijing 100190, China;*
[2]*School of Engineering Science, University of Chinese Academy of Sciences, Beijing 100049, China;*
[3]*Gas Turbine Research Institute/School of Mechanical Engineering, Shanghai Jiao Tong University, Shanghai 200240, China*

Global heat flux measurement techniques with high spatial resolution are needed to accurately capture the peak heat flux and its location for the design of thermal protection system. However, background radiation from combustion presents an obstacle to the application of global heat flux measurement techniques. To solve this problem, a new method for heat flux determination suitable for strong combustion radiation environment is described. The core idea of this method is that heat flux on the inner surface of the combustor was identified by solving the three-dimensional transient inverse heat conduction problem while measuring the outer surface temperature using temperature-sensitive paint. Measurement system configuration, data processing method, and effect of layer thickness of the temperature-sensitive paint on the measurement results are introduced in detail. Finally, both numerical and experimental results are presented to demonstrate the validity of the new method.

**Temperature-sensitive paint, Heat flux, Conjugate gradient method, Air-breathing hypersonic vehicle, Inverse heat conduction problem**

## 1.    Introduction

Air-breathing hypersonic vehicle can reduce the cost of space exploration by using air from the atmosphere for combustion, and have many features that rockets do not, such as hypersonic cruising ability and recoverable space launches. Great strides have been made in the design and development of air-breathing hypersonic, but fundamental research is still required to optimize their operation and performance. One important research area is the quantification of the extreme heat loads caused by combustion heat release [1], since heat flux distribution and location of peak heat flux are critical design parameters to optimize efficiency of the thermal protection system. Many techniques have been used to measure heat flux, such as thermocouples, direct-write sensors [2],

Gardon heat flux gauges [3], diamond calorimeters [4], and state observer-based method [5], all of which have contributed greatly to the development of air-breathing hypersonic vehicle. However, limited by sensor size and installation space, spatial resolution of the above method is limited and is difficult to accurately capture the peak heat flux and its location, especially for areas with large heat flux gradients and complex heat flux distributions. Global heat flux measurement techniques are needed to overcome the problem.

Temperature-sensitive paint (TSP) are well-known global heat flux measurement techniques, that have been commonly used in hypersonic experiments to measurement heat flux and to visualize boundary layer transition. Their use in high temperature condition, however, has been more constrained and few measurements have been carried out. Background radiation from the heated high temperature gases, either by aero-

dynamic heating or combustion, presents the obstacles to the application of TSP [6, 7].

In this study, a new method of applying TSP in hypersonic test with strong combustion radiation is described. Both numerical and experimental results are presented to demonstrate its validity.

## 2. Method

The conventional TSP technique has to airbrush the paint on the inner surface of the combustor and the luminescence of the paint must pass through the flow field before reaching the imaging camera. In general, the luminescence is weak relative to the radiation of the flow field, and this problem cannot be easily solved by optimized spectral filtering or camera gating. To overcome this problem, the heat flux on the inner surface was identified by solving the three-dimensional transient inverse heat conduction problem (IHCP) while also measuring the outer surface temperature using TSP. A comparison of the conventional TSP method and the proposed method is shown in Fig. 1.

### 2.1 Method of temperature measurement

TSP is a thin polymer layer doped with luminescent molecules whose emission under certain excitation is sensitive to temperature due to thermal quenching. The quenching processes can be described using an Arrhenius formulation,

$$\ln \frac{I(T)}{I(T_{\text{ref}})} = \frac{E_a}{R}\left(\frac{1}{T} - \frac{1}{T_{\text{ref}}}\right), \tag{1}$$

where $E_a$ is the activation energy for the non-radiative process, $R$ is the Universal gas constant, $I_{\text{ref}}$ is the emission intensity of the TSP layer at reference temperature $T_{\text{ref}}$. In practise, Eq. (1) does not always hold exactly, so that one tends to carry out a calibration at known $T$ and perform a fit of $I(T)/I(T_{\text{ref}})$ to $T/T_{\text{ref}}$:

$$\frac{I(T_{\text{ref}})}{I(T)} = f(T/T_{\text{ref}}). \tag{2}$$

Therefore, once TSP on a surface is calibrated, the surface temperature can be measured by detecting the luminescent emission from the TSP layer with digital cameras [8-10].

To withstand heat and pressure loads, combustor models is always made of metal or metal alloys such as steel. However, the TSP is an insulator with a thermal conductivity several orders of magnitude lower than that of the steel wall of a combustor. This difference in thermal conductivity requires the use of a double-layer thermal conduction model. Figure 2 shows the thermal conduction model and its corresponding
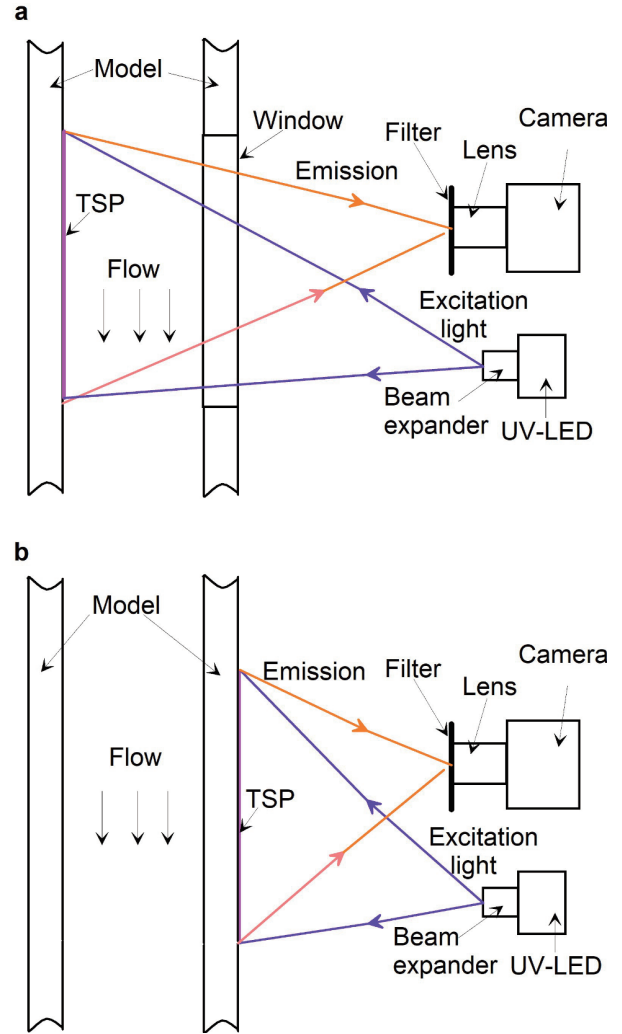


**Figure 1** Comparison of the two methods. **a** Conventional TSP technique; **b** method used in this study.
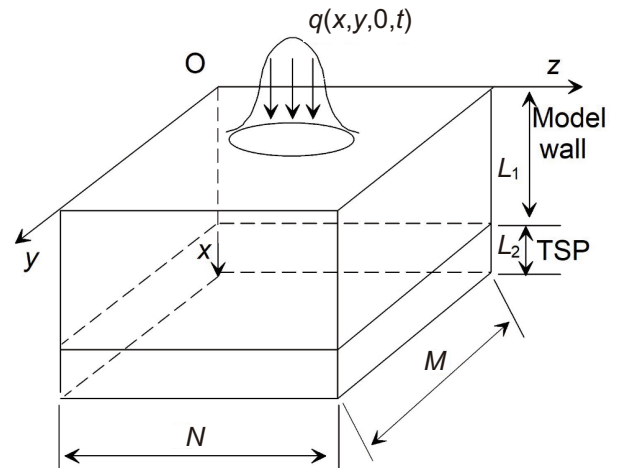


**Figure 2** Double-layer thermal conduction model and its corresponding coordinates.

coordinates. $L_1$ and $L_2$ are the thickness of the test model wall and the TSP layer, respectively. The boundary condi-

tions at the interface of the wall and the TSP layer are based on two requirements: (1) the two layers in contact must have the same temperature at the interface, and (2) the interface must not store any energy, so that the heat flux on both sides of the interface is the same.

## 2.2 Solution of inverse heat conduction problem

With the temperature data measured by TSP, the next step is to solve the IHCP. Well-know methods for solving the IHCP include Tikhonov's regularization method, the conjugate gradient method (CGM), the sequential function specification method, and the Kalman filter method [11]. In this study, the heat flux on the inner surface is recovered by the CGM due to its fast convergence rate and robustness. The CGM is an iterative method and converges the following objective function to a minimum:

$$J[\mathbf{q}(y, z, t)] = \int_0^{t_f} \sum_{i=1}^{im} [\mathbf{T}(x_i, y_i, z_i, t) - \mathbf{Y}(x_i, y_i, z_i, t)]^2 \mathrm{d}t$$

$$= \int_0^{t_f} \sum_{i=1}^{im} [\mathbf{T}_i(t) - \mathbf{Y}_i(t)]^2 \mathrm{d}t, \qquad (3)$$

where $\mathbf{q}(y, z, t)$ is the heat flux on the inner surface, $\mathbf{T}$ and $\mathbf{Y}$ are the calculated and measured temperatures, respectively, of the outer surface at the extracted locations $(x_i, y_i, z_i)$ at time $t$; $im$ represents the number of measured temperature extraction points; and $t_f$ is the final time. The iterative process of CGM to find the heat flux on the inner surface satisfying the temperature of the outer surface was as follows [12-14]:

$$\mathbf{q}^{n+1}(y, z, t) = \mathbf{q}^n(y, z, t) - \beta^n \mathbf{P}^n(y, z, t), \quad n = 0, 1, 2, \ldots, \quad (4)$$

where $n$ is the number of iteration; $\beta^n$ is the search step size form iteration $n$ to $n + 1$; $\mathbf{P}^n$ is the search direction given by the following conjugate equation:

$$\mathbf{P}^n(y, z, t) = \mathbf{J}'^n(y, z, t) + \gamma^n \mathbf{P}^{n-1}(y, z, t), \qquad (5)$$

which is a conjugation of the gradient direction $\mathbf{J}'^n(y, z, t)$ at iteration $n$ and the direction of descent $\mathbf{P}^{n-1}(y, z, t)$ at the iteration $n - 1$. The conjugate coefficient $\gamma^n$ is determined from

$$\gamma^n = \frac{\int_0^{t_f} \sum_{i=1}^{im} [\mathbf{J}'^n(y_i, z_i, t)]^2 \mathrm{d}t}{\int_0^{t_f} \sum_{i=1}^{im} [\mathbf{J}'^{n-1}(y_i, z_i, t)]^2 \mathrm{d}t} \quad \text{with} \quad \gamma^0 = 0. \qquad (6)$$

If the measured temperature of the outer surface contains no errors or noises, the traditional convergence criterion is specified as

$$J[\mathbf{q}(y, z, t)] < \varepsilon, \qquad (7)$$

where $\varepsilon$ is a small-specified number. However, in actual experiment measurement errors is unavoidable and it can be expressed as follows:

$$\mathbf{T}_i(t) - \mathbf{Y}_i(t) \approx \sigma, \qquad (8)$$

where $\sigma$ is the stand deviation of measurements. Substituting Eq. (8) into Eq. (3), the following expression for $\varepsilon$ is obtained:

$$\varepsilon = im\sigma^2 t_f. \qquad (9)$$

To perform the iterative process of CGM method, the calculated temperature $\mathbf{T}_i$, the search step size $\gamma^n$, and the search direction $\mathbf{P}^n$ are needed. In order to develop expressions for the determination of these three quantities, a direct heat conduction problem, a sensitivity problem, and an adjoint problem are constructed as described below.

(1) Heat conduction problem

In the direct heat conduction problem, heat flux of the inner surface is known, and the temperatures of the outer surface are determined from the solution of the mathematical formulation, given as follows:

$$\frac{\partial \mathbf{T}}{\partial t} = \alpha \left( \frac{\partial^2 \mathbf{T}}{\partial x^2} + \frac{\partial^2 \mathbf{T}}{\partial y^2} + \frac{\partial^2 \mathbf{T}}{\partial z^2} \right), \qquad (10a)$$

$$-k\frac{\partial \mathbf{T}}{\partial x} = q(y, z, t) \quad \text{for} \quad x = 0, \quad t > 0, \qquad (10b)$$

$$-k\frac{\partial \mathbf{T}}{\partial x} = 0 \quad \text{for} \quad x = L, \quad t > 0, \qquad (10c)$$

$$-k\frac{\partial \mathbf{T}}{\partial y} = 0 \quad \text{for} \quad y = 0, M, \quad t > 0, \qquad (10d)$$

$$-k\frac{\partial \mathbf{T}}{\partial z} = 0 \quad \text{for} \quad z = 0, N, \quad t > 0, \qquad (10e)$$

$$\mathbf{T} = T_0 \quad \text{for} \quad 0 \le x \le L, \quad 0 \le y \le M,$$
$$0 \le z \le N, \quad t = 0, \qquad (10f)$$

where, $k$ and $\alpha$ are the thermal conductivity and thermal diffusivity of the material; $L$, $M$, and $N$ are the size of the wall in the $x$, $y$, $z$ direction, respectively. The initial temperature of the wall is uniform and equals $T_0$. The heat flux on the inner surface is a function of time as well as $y$ and $z$ distances. All side wall surfaces and the outer surface are assumed to be adiabatic.

(2) Sensitivity problem and search step size

Sensitivity problem can be obtained by the limiting approach. When $\mathbf{q}$ is perturbed by $\Delta\mathbf{q}$, temperature $\mathbf{T}$ undergoes a variation of $\Delta\mathbf{T}$. Plugging $\mathbf{q} + \Delta\mathbf{q}$ and $\mathbf{T} + \Delta\mathbf{T}$ into Eq. (10a), subtracting the Eq. (10a) and neglecting the second-order terms, the following sensitivity function $\Delta\mathbf{T}$ can be obtained:

$$\frac{\partial \Delta\mathbf{T}}{\partial t} = \alpha \left( \frac{\partial^2 \Delta\mathbf{T}}{\partial x^2} + \frac{\partial^2 \Delta\mathbf{T}}{\partial y^2} + \frac{\partial^2 \Delta\mathbf{T}}{\partial z^2} \right), \qquad (11a)$$

$$-k\frac{\partial \Delta\mathbf{T}}{\partial x} = \Delta\mathbf{q}(y, z, t) \quad \text{for} \quad x = 0, \quad t > 0, \qquad (11b)$$

$$-k\frac{\partial \Delta \mathbf{T}}{\partial x} = 0 \quad \text{for} \quad x = L, \quad t > 0, \tag{11c}$$

$$-k\frac{\partial \Delta \mathbf{T}}{\partial y} = 0 \quad \text{for} \quad y = 0, M, \quad t > 0, \tag{11d}$$

$$-k\frac{\partial \Delta \mathbf{T}}{\partial z} = 0 \quad \text{for} \quad z = 0, N, \quad t > 0, \tag{11e}$$

$$\Delta \mathbf{T} = 0 \quad \text{for} \quad 0 \le x \le L, \quad 0 \le y \le M,$$
$$0 \le z \le N, \quad t = 0. \tag{11f}$$

With the solution of the sensitivity equation, the search step size $\beta^n$ can be determined by Eq. (12) as follows:

$$\beta^n = \frac{\int_0^{t_f} \sum_{i=1}^{im} [\mathbf{T}_i(t) - \mathbf{Y}_i(t)] \Delta \mathbf{T}_i(t) \mathrm{d}t}{\int_0^{t_f} \sum_{i=1}^{im} [\Delta \mathbf{T}_i(t)]^2 \mathrm{d}t}. \tag{12}$$

(3) Adjoint problem and gradient equation

To obtain the adjoint problem, multiplying Eq. (10a) by Lagrange multiplier $\lambda$ and integrating the result over the time and spatial domain then adding the integration result to the right-hand-size of Eq. (3), the functional $J$ can be rewritten as

$$J[\mathbf{q}(y,z,t)] = \int_0^{t_f} \sum_{i=1}^{im} [\mathbf{T}_i(t) - \mathbf{Y}_i(t)]^2 \mathrm{d}t$$
$$+ \int_0^{t_f} \int_\Omega \left\{ \frac{\partial}{\partial x}\left(k\frac{\partial \mathbf{T}}{\partial x}\right) + \frac{\partial}{\partial y}\left(k\frac{\partial \mathbf{T}}{\partial y}\right) \right.$$
$$\left. + \frac{\partial}{\partial z}\left(k\frac{\partial \mathbf{T}}{\partial z}\right) - \rho c \frac{\partial \mathbf{T}}{\partial t} \right\} \lambda \mathrm{d}x\mathrm{d}y\mathrm{d}z\mathrm{d}t \tag{13}$$

with limiting process of Eq. (13), the adjoint problem can be obtained

$$\rho c \frac{\partial \lambda}{\partial t} + \frac{\partial^2 \lambda}{\partial x^2} + \frac{\partial^2 \lambda}{\partial y^2} + \frac{\partial^2 \lambda}{\partial z^2} = 0, \tag{14a}$$

$$-k\frac{\partial \lambda}{\partial x} = 0 \quad \text{for} \quad x = 0, \quad t > 0, \tag{14b}$$

$$-k\frac{\partial \lambda}{\partial x} = -2(\mathbf{T} - \mathbf{Y})\delta(x - x_i)\delta(y - y_i)\delta(z - z_i)$$
$$\text{for} \quad x = L, \quad t > 0, \tag{14c}$$

$$-k\frac{\partial \lambda}{\partial y} = 0 \quad \text{for} \quad y = 0, M, \quad t > 0, \tag{14d}$$

$$-k\frac{\partial \lambda}{\partial z} = 0 \quad \text{for} \quad z = 0, N, \quad t > 0, \tag{14e}$$

$$\lambda = 0 \quad \text{for} \quad 0 \le x \le L, \quad 0 \le y \le M,$$
$$0 \le z \le N, \quad t = t_f, \tag{14f}$$

where $\delta(\cdot)$ is the Dirac $\delta$ function. Eq. (13) can be simplified as

$$\Delta J[\mathbf{q}(y,z,t)] = \int_{z=0}^{N} \int_{y=0}^{M} \int_{t=0}^{t_f} \lambda(0,y,z,t)\Delta \mathbf{q}(y,z,t)\mathrm{d}t\mathrm{d}y\mathrm{d}z. \tag{15}$$

The variation of functional can be written as

$$\Delta J[\mathbf{q}(y,z,t)] = \int_{z=0}^{N} \int_{y=0}^{M} \int_{t=0}^{t_f} \mathbf{J}'[q(y,z,t)]\Delta \mathbf{q}(y,z,t)\mathrm{d}t\mathrm{d}y\mathrm{d}z. \tag{16}$$

A comparison of Eqs. (15) and (16) leads to the result for the gradient of functional:

$$\mathbf{J}'[q(y,z,t)] = \lambda(0,y,z,t). \tag{17}$$

To solve the direct heat conduction problem, sensitivity problem, and adjoint problem numerically, a finite difference code was developed based on the alternating direction implicit (ADI) method. The ADI method applies the Crank-Nicolson method one direction at a time using two intermediate temperature fields before obtaining the new temperature field. All three iterations for $x$, $y$, and $z$ directions have to done for each time step. The numerical errors of ADI solution are in the order of $O((\Delta t)^2)$ and $O((\max[\Delta x, \Delta y, \Delta z])^2)$. For the adjoint problem, the final time conditions at time $t = t_f$ is specified instead of the customary initial condition. This problem can be transformed to an initial problem by the transformation of the time variables. Then all the three problems can be solved by the same finite difference code.

The computational procedure of the CGM method is summarized as follows. Firstly, the direct heat conduction problem is computed based on the guesses of the inner surface heat flux to obtain the outer surface temperature $\mathbf{T}$. Afterwards, by comparing this temperature with the measured one, $\mathbf{Y}$, the objective function is evaluated. If the convergence criterion is not reach, a new inner surface heat flux is computed by solving the sensitivity and adjoint problem. This process is iterated until the convergence criterion is satisfied.

## 3.   Numerical validation

In this section, validity of the CGM in estimating the inner surface heat flux from inverse analysis of the outer surface temperature is demonstrated. The first step of the validation was to impose a known heat flux on the inner surface of the scramjet wall and record the outer surface temperature change. This temperature was then the input for the CGM as TSP measured results. Finally, the estimated heat flux was compared with the imposed heat flux to evaluate the validity of the approach.

The geometry of the test case is a plate that represents part of a combustor wall with thickness in the $x$-direction, the outer surface of which is painted with TSP. The material of the plate is C45E4 steel, and its length and width are 90 and 60 mm, respectively. The density, specific heat, and thermal conductivity of the C45E4 steel and the TSP are 7870 and 1300 kg m$^{-3}$, 486 and 1540 J kg$^{-1}$ K$^{-1}$, and 51.9 and 0.16 W m$^{-1}$ K$^{-1}$, respectively. The test time was set to be 2 s. The unknown heat flux on the inner surface was assumed to be

$$q(y,z) = q_0 \left[ 1 + 0.2 \sin\left(\frac{\pi y}{45}\right) \right] f(z), \tag{18}$$

where $q_0$ equals 0.4 MW/m². The $f(z)$ function simulates the boundary condition of the combustor wall, and is defined as follows:

$$f(z) = \begin{cases} \sin\left(\dfrac{2\pi}{54}z\right), & 0 \leq z < 13.5, \\ 1.0, & 13.5 \leq z < 46.8, \\ \sin\left[\dfrac{2\pi}{54}(z - 33.3)\right], & 46.8 \leq z \leq 60. \end{cases} \quad (19)$$

To ensure that the temperature of the outer surface was within the measuring range of the TSP, the thickness of the plate was set to 5.1 mm. The thickness of the TSP layer was set to a typical value of 20 μm.

An analytical solution can be obtained when the heat flux on the inner surface is constant, which can then be used to study the grid independence. The time step was set to 5.0 μs and the grids along the $y$ and $z$ directions were set to 0.3 mm. The $x$ direction grids of the plate and the TSP layer were 0.3 mm and 2.0 μm, respectively. The computational domain wss assumed to be at the uniform temperature of 288 K initially. With these parameters, the direct heat conduction problem can be solved to obtain the outer surface temperature change, which is regarded as the TSP measured results. The CGM was used to recover the heat flux on the inner surface. The CGM was first performed by assuming exact temperature data. To generate results for situations involving measurement errors, Normally distributed random errors within the range of ±1.0 and ±3.0 K were added to the temperature data. In all of the cases considered herein, the initial estimates of the inner surface heat flux were taken to be zero. Figure 3 shows the solutions given by the CGM with different levels of temperature noise. The input temperature with noise was filtered using a 2D averaging filter of size 11 by 11 points. As shown in Fig. 3, reliable estimations were obtained when using both exact temperatures and temperatures with noise. To analyze the results quantitatively, the exact heat flux ($q_E$) and the CGM solutions ($q_{CGM}$) at $z = 30$ mm were compared in Fig. 4.

As shown in Fig. 4, differences between the exact heat flux and the CGM solutions can be observed, and the relative error increases with the temperature noise. However, the relative error values of the inner surface heat flux are all less than 3%, which demonstrates the high accuracy of the proposed method.

Figure 5 shows the convergence process of the CGM. The convergence process was stopped when the difference between the calculated temperature and measured temperature reached less than 0.5 K. Convergence was reached after 9 iterations for the above cases. The figure shows the following: (1) The function decreases rapidly for the first few iterations, indicating that the initial estimates of the unknown quantities
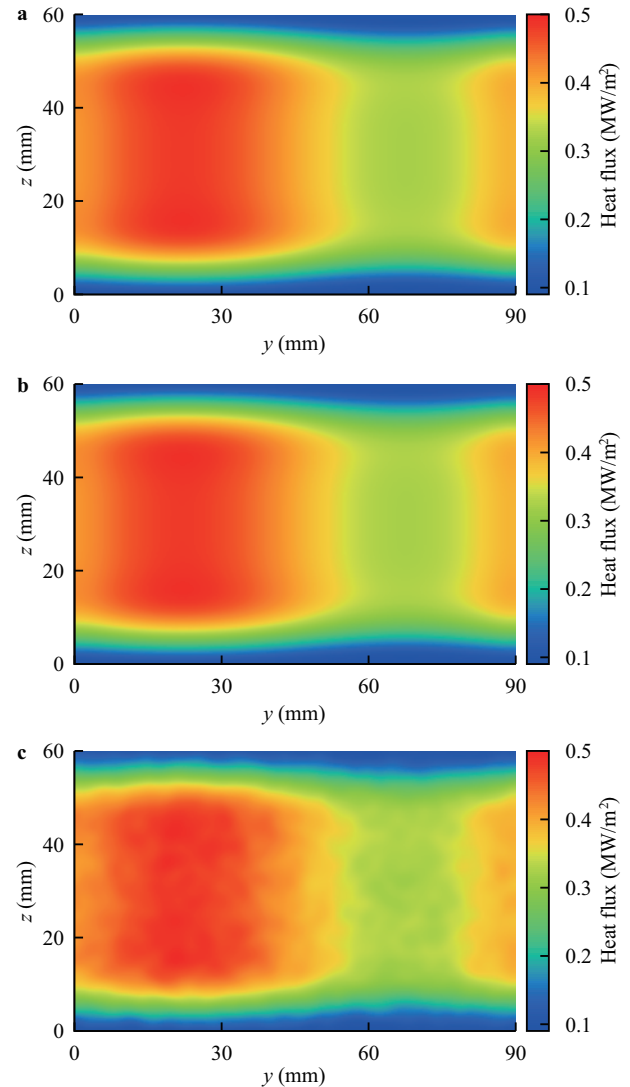


**Figure 3** CGM solution. **a** Without temperature noise; **b** with a temperature noise of ±1.0 K; **c** with a temperature noise of ±3.0 K.

can be chosen arbitrarily. If a difference of 0.7 K is acceptable, then only 3 iterations are required to reach convergence. These features make the CGM easy to use in practical applications. (2) The convergence curves with and without noise are nearly the same, indicating that the CGM is robust and applicable to solve the IHCP.

The numerical results show that the heat flux can be accurately determined by the CGM with a double-layer thermal conduction model. Theoretically, the thickness of the TSP layer should be determined before analysis. However, in practice, the TSP layer may be uneven, as it is difficult to control its thickness, especially on complex surface models. Hence, the effect of TSP layer thickness on the accuracy of heat flux measurements must be studied. To make the analysis results more generalizable, limited conditions were considered, wherein the thickness of the TSP layer was considered to be zero and the CGM was conducted with a single-
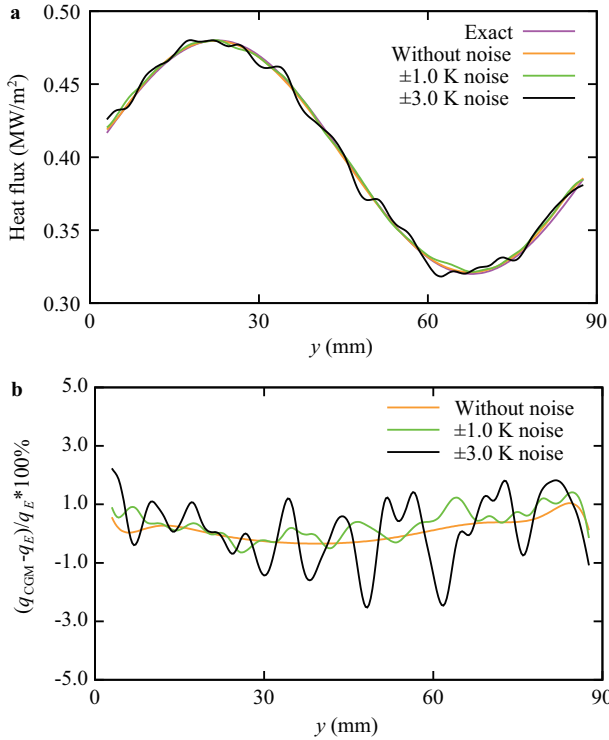
**Figure 4** Comparison of the exact heat flux and CGM solution with different level of noise ($z$ = 30 mm). **a** CGM solution; **b** relative error.
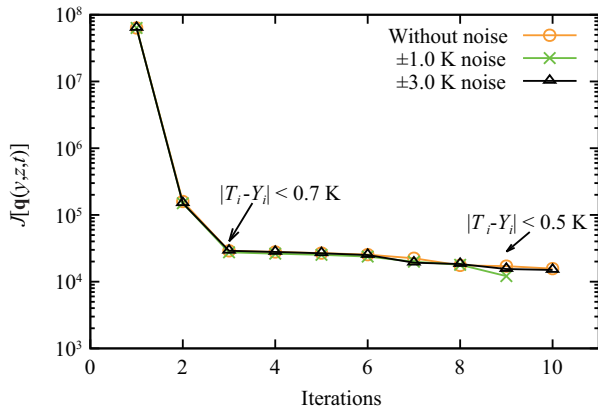


**Figure 5** Convergence process.

layer thermal conduction model. Numerical cases with different TSP layer thicknesses, test model wall thicknesses, wall materials, and heat flux environments were performed, the results of which are shown in Fig. 6. The quantitative effects of ignoring the TSP layer thickness are summarized in Table 1. The time needed for a $q_{CGM}$ of 90% of $q_E$ and a value of $\frac{q_{CGM}}{q_E}$ with a test time of 2 s is also listed. The following observations can be made from the results: (1) when the TSP layer thickness is not considered, the CGM solution ($q_{CGM}$) is lower than the exact value, because due to the relatively low thermal conductivity of the TSP, the temperature gradient of the TSP layer is much higher than that of the test

model wall, and the outer surface temperature is lower than is the case when the TSP layer is absent. (2) The critical time is defined as the time when the outer surface temperature begins to change approximately linearly. An increase in the TSP layer or model wall thickness, or the selection of a material with a relatively low thermal diffusivity, prolongs the critical time and the relative error increases slightly. (3) The relative error of $q_{CGM}$ does not decrease infinitely with the test time, but is limited. When the test time is longer than the critical time, the relative error of the $q_{CGM}$ approaches the limit. For all of the cases considered here, when the test time is equal to 2 s, the relative errors are all less than 4.0%. Therefore, ignoring the TSP layer thickness is practically acceptable as long as the test time is longer than the critical time.

## 4. Experimental results

### 4.1 Scramjet

The proposed method was firstly tested at a variable Mach number direct-connect supersonic combustion test facility, which consists of the heater, sonic nozzle, isolation section, combustor, and exhaust nozzle. The TSP was sprayed onto the exhaust nozzle of the scramjet, namely, a unilateral expansion nozzle with an expansion angle of 2.0°. Figure 7 is a photograph of the facility. Detailed information of the facility and test model are available in Ref. [15]. For the experiments reported here, the Mach number, stagnation pressure, and stagnation temperature of the inlet were 2.8, 1.68 MPa, and 1475 K, respectively. The inlet conditions were representative of Mach 5.6 flight conditions with a dynamic pressure of 64 kPa. The fuel was ethylene and was injected after the supersonic flow in the scramjet had well developed.

In the experiments, an oxygen-impermeable automobile clearcoat was used as the binder, and Ru(dpp) was used as the luminophore of the TSP. The absorption and emission spectra of the TSP used in the tests can be found in Ref. [16]. The TSP was air-sprayed onto the model surface and the resulting paint thickness was approximately 20 μm. Continuous illumination was provided by a 455 nm LED. The luminescence signal was recorded continuously by a 12-bit high-speed camera (SA-4, Photron) at 250 Hz through a 60 mm lens, and the size of the raw images was 1024 by 1024 pixels. The spatial resolution for the tests are 0.32 mm. A 600 ± 25 nm band-pass filter was selected to exclude excitation light. The temperature calibration of the TSP was performed in a calibration device with a temperature range of 298-318 K. As shown in Fig. 8, a nonlinear relationship was found between intensity and temperature, that could be fitted by a polynomial curve.
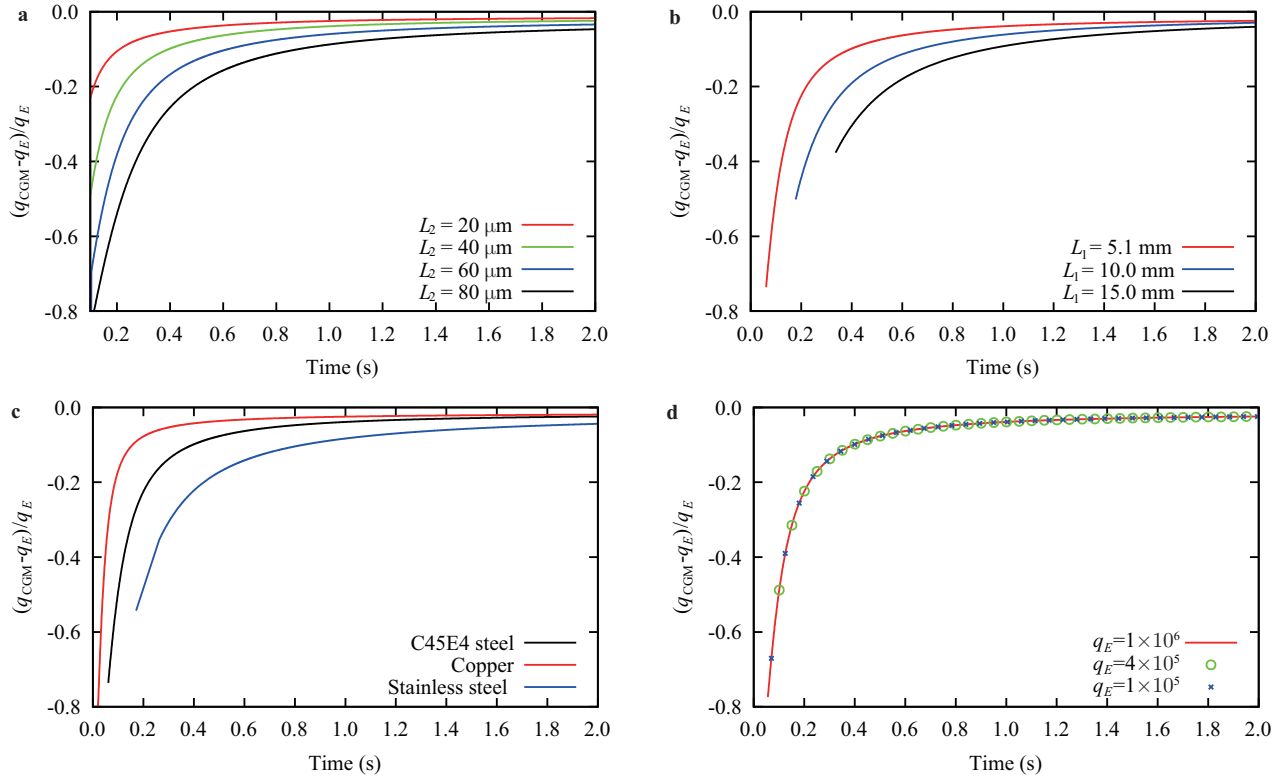
**Figure 6** Effects of ignoring the TSP layer thickness on the measurement results. **a** Thickness of the TSP layer ($L_1$ = 5.1 mm, C45E4 steel, $q_E$ = 4× $10^5$ W/m$^2$); **b** thickness of the test model wall ($L_2$ = 40 μm, C45E4 steel); **c** test model material ($L_1$ = 5.1 mm, $L_2$ = 40 μm, $q_E$ = 4 × $10^5$ W/m$^2$); **d** heat flux values ($L_1$ = 5.1 mm, $L_2$ = 40 μm, C45E4 steel).

**Table 1**　Quantitative effects of ignoring the TSP layer thickness

| $L_1$ (mm) | $L_2$ (μm) | Material | $q_E$ (W/m$^2$) | Time (s) ($q_{CGM} = 0.9q_E$) | $q_{CGM}/q_E$ (time = 2 s) |
|---|---|---|---|---|---|
| 5.1 | 20 | C45E4 steel | 4 × $10^5$ | 0.211 | 0.983 |
| 5.1 | 40 | C45E4 steel | 4 × $10^5$ | 0.394 | 0.976 |
| 5.1 | 60 | C45E4 steel | 4 × $10^5$ | 0.618 | 0.966 |
| 5.1 | 80 | C45E4 steel | 4 × $10^5$ | 0.883 | 0.954 |
| 10.0 | 40 | C45E4 steel | 2 × $10^6$ | 0.665 | 0.971 |
| 15.0 | 40 | C45E4 steel | 1 × $10^7$ | 0.938 | 0.960 |
| 5.1 | 40 | Copper | 4 × $10^5$ | 0.157 | 0.981 |
| 5.1 | 40 | Stainless steel | 4 × $10^5$ | 0.833 | 0.967 |
| 5.1 | 40 | C45E4 steel | 1 × $10^6$ | 0.394 | 0.976 |
| 5.1 | 40 | C45E4 steel | 1 × $10^5$ | 0.394 | 0.976 |

　　Figure 9a shows the measured temperature distribution with a test time of 7.8 s. The flow in the figures are from right to left. The outer surface temperature of the scramjet wall was measured and the distribution of the heat flux was obtained using the CGM, as shown in Fig. 9b. At present, few numerical and experimental results are available for cross-validation. Considering that the heat flux distribution should reflect the geometric characteristics of the test model, positions of the upper and lower wall of the nozzle were extracted. Points on the wall with a heat flux equal to 10% of the maximum heat flux were defined as representing the wall boundary. The red and black lines in Fig. 9b show the results. The position data was further analyzed using the least square method. The fitted included angle of the upper and lower wall boundary is 2.1°, which agrees well with the test model. Further tests were conducted with varying fuel-air equivalence ratios. The resulting heat flux distributions were similar to these in Fig. 9b. A comparison of the heat flux with different equivalence ratios along $y$ = 100 mm is shown in Fig. 10. The figure clearly shows that an increase in the
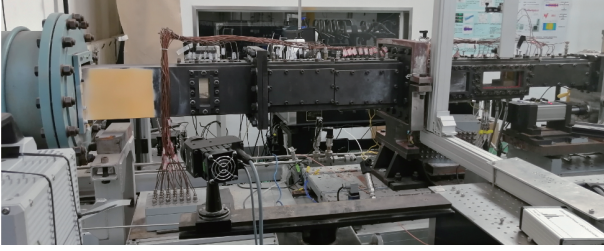
**Figure 7** Photograph of the direct-connect supersonic combustion test facility.
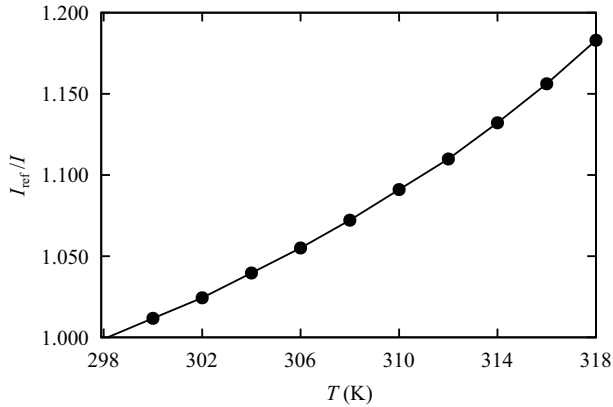


**Figure 8** TSP calibration results.

equivalence ratio increased the heat flux but had little effect on the heat flux distribution.

## 4.2 Oblique detonation engine

Further tests were carried out in the JF-12 shock tunnel with an oblique detonation engine (ODE) to verify its feasibility in pulse wind tunnels with short test time. The JF-12 shock tunnel is capable of reproducing airflow for Mach numbers ranging from 5 to 9 at an altitude of 25-50 km, with a test duration of about 100 ms [17]. The ODE model, shown in Fig. 11, is about 2.2 m in length, 0.6 m in height and 0.6 m in width. It is mainly composed of fuel injectors, inlet, combustor and nozzle. The combustor is in the shape of a rectangular straight channel, which is 0.0765 m in height and 0.4 m in width. The fuel was hydrogen and the global equivalence ratio of the fuel-air mixture flowing into the combustor is about 1.0. More information of the test model can be found in Ref. [18].

The time for heat to penetrate to the outer surface of the combustor is defined as the heat penetration time. The analytical expression for heat penetration time is

$$t_p = \frac{L^2}{\alpha \pi^2} \ln(2), \tag{20}$$

where $L$ is the wall thickness and $\alpha$ is the thermal diffusivity of the material. The combustor is make of carbon structural

steel and its thickness is 8 mm. The heat penetration time is much longer than the test time (100 ms). Thermal diffusivity of copper and carbon structural steel is $1.15 \times 10^{-4}$ m$^2$/s
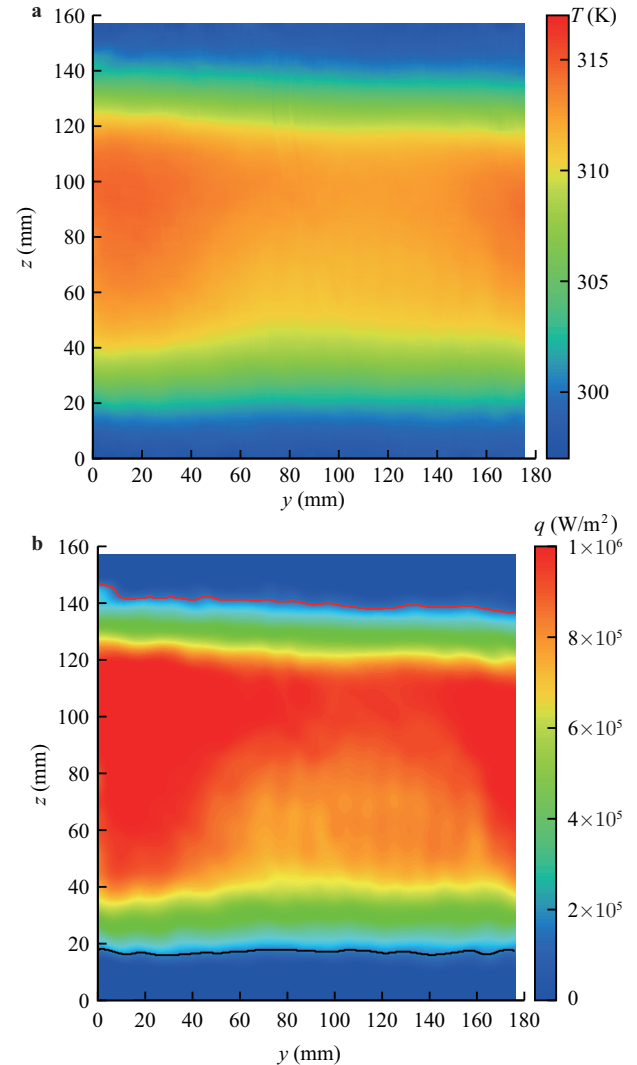


**Figure 9** Measured temperature and heat flux distribution identified by the CGM. **a** Measured temperature ($t = 7.8$ s); **b** heat flux distribution.



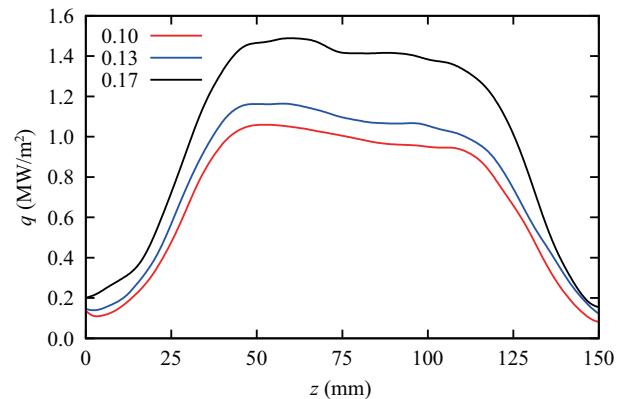**Figure 10** Heat flux distribution with different equivalence ratios ($y = 100$ mm).

and $1.36 \times 10^{-5}$ m$^2$/s, respectively. Hence, to meet the demand of the test time, the TSP was air-sprayed onto a copper sheet. Its thickness is 1.0 mm and the corresponding heat penetrate time equals to 0.61 ms. Then, the copper sheet was flush-mounted on the the combustor, with an optical glass to isolate the TSP from the external flow field. In Fig. 11, TSP is indicated by bright yellow color.

Figure 12 shows the measured heat flux distribution of the ODE combustor. The spatial resolution for this test is 0.33 mm. Flow in the figure are from right to left. The high heat flux region on the right side of the figure is caused by the oblique detonation wave while the left one is caused by the reflected shock wave. Although the combustor is two dimensional, the high heat flux regions are non-uniform along $z$ direction due to the non-uniformity of fuel injection.

Four coaxial thermocouples with a diameter of 1.4 mm was used to validate the new method. The thermocouple is self-developed and has been widely used in high temperature pulse wind tunnels. Its sensitivity depends on material, and is a constant for our experimental conditions. The sensitivity has been well calibrated for each batch of material before every test. The thermocouples were stuck in the mounting hole of the the combustor with glue. The heat flux measured by thermocouples are 0.69, 1.05, 0.77, and 0.78 WM/m$^2$, respectively. Heat flux distribution extracted from Fig. 12 with $y = 126$ mm and results measured by thermocouples were compared in Fig. 13. As shown in the figure, the heat flux measured by TSP varies between 0.73 and 0.90 WM/m$^2$. The results between TSP and thermocouples at the same cross-section are compared considering the two-dimensionality of ODE combustor. The comparison shows that although there are some differences (probably due to the nonuniformity of fuel injection), the TSP results are generally close to the thermocouples in the magnitude. The difference between the mean results for TSP and thermocouples is smaller than 8.2%, which demonstrates the feasibility of the new method.

## 5.    Conclusion

A new method of applying TSP in hypersonic test with strong combustion radiation is proposed. The heat flux on the inner surface of the combustor is determined by recording the development of the outer surface temperature of the wall using TSP and then solving the IHCP. Background radiation can be avoided for the TSP is physically isolated from the combustion flow. Numerical and experimental tests were conducted to validate this method, and the following conclusions can be derived: (1) The CGM method can be applied to solve the three-dimensional IHCP considering noise with great
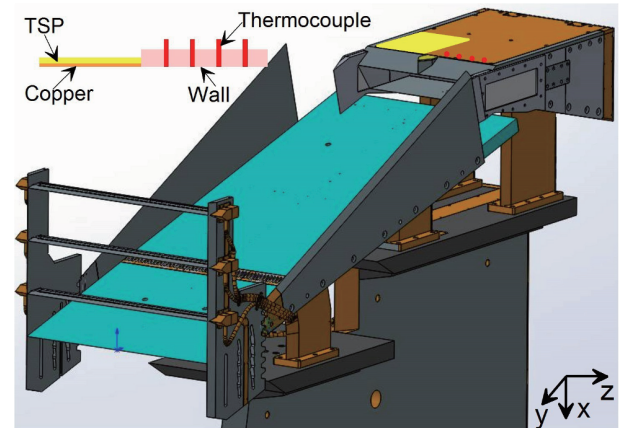


**Figure 11**    ODE model (the bright yellow region represents TSP, while the red dots indicate the location of the thermocouples).
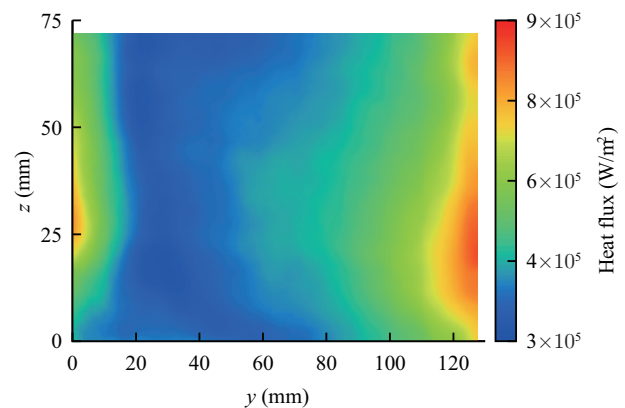


**Figure 12**    Measured heat flux distribution of the ODE combustor.
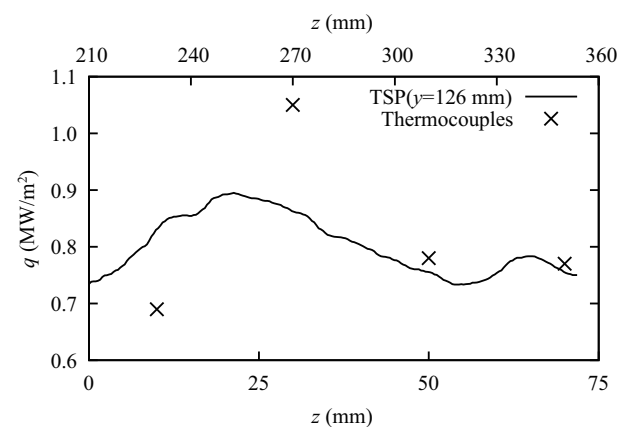


**Figure 13**    Comparison of heat flux measured by TSP and thermocouples (results measured with TSP were plotted with the bottom $z$-axis, while results obtained by thermocouples were plotted with the top $z$-axis).

accuracy, robustness and convergence. (2) Simplification to single-layer heat conduction problem by ignoring the thin TSP layer will bring computational convenience but also some errors. Nevertheless, the error is relatively small when

the test time is longer than the critical time. (3) Two typical experimental cases with long test time and short test time demonstrates the feasibility of the method qualitatively and quantitively, respectively. The results in the direct-connection supersonic combustion test facility show the heat flux field in the exhaust nozzle with high spatial resolution and its variance with equivalence ratios. The results in ODE show the satisfactory coincidence between the TSP and thermocouple with the mean difference of 8.2%.

1. P. Kennedy, J. Donbar, J. Trelewicz, C. Gouldstone, and J. Longtin, in Heat flux measurements in a scramjet combustor using direct write technology: Proceedings of the 17th AIAA International Space Planes and Hypersonic Systems and Technologies Conference, San Francisco, 2012.

2. J. R. Trelewicz, J. P. Longtin, C. Gouldstone, P. J. Kennedy, and J. M. Donbar, Heat flux measurements in a scramjet combustor using embedded direct-write sensors, J. Propuls. Power **31**, 1003 (2015).

3. M. Goldfeld, The heat flux research in hydrogen supersonic combustor at Mach number of 4, Int. J. Hydrogen Energy **46**, 13365 (2021).

4. R. T. P. Geraets, M. McGilvray, L. J. Doherty, R. G. Morgan, C. M. James, and D. R. Buttsworth, Development of a fast-response diamond calorimeter heat transfer gauge, J. Thermophys. Heat Transfer **34**, 193 (2020).

5. C. Zhang, J. Qin, Q. Yang, S. Zhang, J. Chang, and W. Bao, Indirect measurement method of inner wall temperature of scramjet with a state observer, Acta Astronaut. **115**, 330 (2015).

6. W. H. Beck, C. Klein, U. Henne, J. M. Schramm, A. Wagner, K. Hannemann, T. Gawehn, and A. Guelhan, in Application of temperature and pressure sensitive paints to DLR hypersonic facilities: "Lessons learned": Proceedings of the 53rd AIAA Aerospace Sciences Meeting, Kissimmee, 2015.

7. D. Peng, and Y. Liu, Fast pressure-sensitive paint for understanding complex flows: From regular to harsh environments, Exp. Fluids **61**, 8 (2020).

8. D. Peng, X. Liu, L. Jiao, Z. Li, X. Wen, C. Yuan, G. Han, Y. Liu, Y. Liu, and Z. Jiang, Noise reduction for temperature-sensitive paint measurement contaminated by strong background radiation in a high enthalpy hypersonic tunnel, Acta Mech. Sin. **37**, 20 (2021).

9. T. Liu, J. Montefort, N. Schick, S. Stanfield, S. Palluconi, and J. Crafton, Correction for effect of temperature-dependent diffusivity on temperature-sensitive-paint heat-flux measurement, Int. J. Heat Mass Transfer **137**, 337 (2019).

10. S. Risius, W. H. Beck, C. Klein, U. Henne, and A. Wagner, Determination of heat transfer into a wedge model in a hypersonic flow using temperature-sensitive paint, Exp. Fluids **58**, 117 (2017).

11. P. Xiong, J. Deng, T. Lu, Q. Lu, Y. Liu, and Y. Zhang, A sequential conjugate gradient method to estimate heat flux for nonlinear inverse heat conduction problem, Ann. Nucl. Energy **149**, 107798 (2020).

12. L. Cheng, F. Zhong, H. Gu, and X. Zhang, Application of conjugate gradient method for estimation of the wall heat flux of a supersonic combustor, Int. J. Heat Mass Transfer **96**, 249 (2016).

13. C. H. Huang, and W. C. Chen, A three-dimensional inverse forced convection problem in estimating surface heat flux by conjugate gradient method, Int. J. Heat Mass Transfer **43**, 3171 (2000).

14. M. Mohammadiun, and A. B. Rahimi, Estimation of the time-dependent heat flux using the temperature distribution at a point by conjugate gradient method, Arab. J. Sci. Eng. **38**, 971 (2013).

15. Y. Meng, H. Gu, and F. Chen, Influence of plasma on the combustion mode in a scramjet, Aerospace **9**, 73 (2022).

16. D. Peng, F. Xie, X. Liu, J. Lin, Y. Li, J. Zhong, Q. Zhang, and Y. Liu, Experimental study on hypersonic shock-body interaction between bodies in close proximity using translucent fast pressure- and temperature-sensitive paints, Exp. Fluids **61**, 120 (2020).

17. C. K. Yuan, and Z. L. Jiang, Experimental investigation of hypersonic flight-duplicated shock tunnel characteristics, Acta Mech. Sin. **37**, 422 (2021).

18. Z. Zhang, C. Wen, C. Yuan, Y. Liu, G. Han, C. Wang, and Z. Jiang, An experimental study of formation of stabilized oblique detonation waves in a combustor, Combust. Flame **237**, 111868 (2022).

# 温敏漆应用于高超声速燃烧辐射环境的方法

苑朝凯, 孟凡钊, 刘旭, 刘云峰, 连欢, 刘应征, 彭迪

**摘要** 热防护系统设计需要高空间分辨率的热流密度场测量方法来获取热流密度峰值及其对应的空间位置. 然而, 燃烧产生的背景辐射严重阻碍了现有热流密度场测量方法的应用. 为了解决该难题, 提出了一种适用于强辐射燃烧环境的热流密度场测量方法, 基本思想是利用温敏漆测量燃烧室外壁面温度的变化历程结合三维瞬态热传导反问题的求解确定内壁面热流密度场分布. 文中详细介绍了测量系统构成、数据处理方法及温敏漆涂层厚度对测量结果的影响, 最后给出了数值和实验结果验证了该方法的可行性.